Inflammasome activation causes dual recruitment of NLRC4 and NLRP3 to the same macro-molecular complex

Si Ming Man,[1] Lee J. Hopkins,[1] Eileen Nugent,[2] Susan Cox,[3] Ivo M. Glück,[1] Panagiotis Tourlomousis,[1] John A. Wright,[1] Pietro Cicuta,[2] Tom P. Monie,[4] Clare E. Bryant[1*]

[1] Department of Veterinary Medicine, University of Cambridge, Madingley Road, CB3 0ES, United Kingdom.

[2] Sector of Biological and Soft Systems, The Cavendish Laboratory, University of Cambridge, Madingley Road, Cambridge

[3] Randall Division of Cell & Molecular Biophysics, Kings College, London, WC2R 2LS

[4] Department of Biochemistry, University of Cambridge, 80 Tennis Court Road, Cambridge, CB2 1GA, United Kingdom.

* Correspondence to:
Clare E. Bryant
Professor of Innate Immunity
Department of Veterinary Medicine,
University of Cambridge,
Madingley Road, CB3 0ES, United Kingdom.
E-mail: ceb27@cam.ac.uk
Phone: +44 (0)1223 766232
Fax: +44 (0)1223 337610

Running Title: NLRC4-NLRP3 inflammasome

Keywords: caspase-1, caspase-8, bacteria, speck, innate immunity

Author contributions: S.M.M., L.J.H., E.N., S.C., I.G., P.T., and J.A.W. performed research; S.M.M., L.J.H., E.N., S.C., P.T., J.A.W., P.C., T.P.M., and C.E.B. analyzed data; and S.M.M., T.P.M., and C.E.B. wrote the paper.

The authors declare no conflict of interest.

Abstract

Pathogen recognition by nucleotide-binding oligomerization domain-like receptor (NLR) results in the formation of a macro-molecular protein complex (inflammasome) that drives protective inflammatory responses in the host. It is thought that the number of inflammasome complexes forms in a cell is determined by the number of NLRs being activated, with each NLR initiating its own inflammasome assembly independently of one another; however, here we show that the important food poisoning bacterium *Salmonella enterica* serovar Typhimurium (*S.* Typhimurium) simultaneously activates at least two NLRs whilst only a single inflammasome complex is formed in a macrophage. Both NLRC4 and NLRP3 are simultaneously present in the same inflammasome where both NLRs are required to drive IL-1β processing within the *Salmonella*-infected cell and regulate the bacterial burden in mice. Super resolution imaging of *Salmonella*-infected macrophages revealed a macro-molecular complex with an outer ring of ASC, an inner ring of NLRs, with active caspase effectors containing the pro-IL-1β substrate localized internal to the ring structure. Our data reveal the spatial localization of different components of the inflammasome and how different members of the NLR family co-operate to drive robust IL-1β processing during *Salmonella* infection.

Significance Statement

The nucleotide oligomerization domain-like receptor (NLR) family members, NLRC4 and NLRP3, activate the inflammasome to provide host defenses against infection. The precise molecular constituents of an inflammasome are unknown, however, it is believed that receptor-specific complexes containing ASC and caspase-1 are formed. Here we used confocal and super-resolution microscopy to show that in macrophages infected with *Salmonella* Typhimurium, a pathogen that activates two distinct NLRs, ASC forms an outer ring-like structure that comprises NLRC4, NLRP3, caspase-1, caspase-8 and pro-IL-1β within the same macro-molecular complex. These results suggest that the inflammasome is a highly dynamic macro-molecular protein complex capable of recruiting different NLRs and effectors to co-ordinate inflammasome responses to infection.

\body

INTRODUCTION

Inflammasomes are cytosolic multimeric protein complexes formed in the host cell in response to the detection of pathogen–associated molecular patterns (PAMPs) or danger–associated molecular patterns (DAMPs). Formation of the inflammasome in response to PAMPs is critical for host defense because it facilitates processing of the proinflammatory cytokines pro-IL-1β and pro-IL-18 into their mature forms (1). The inflammasome also initiates host cell death in the form of pyroptosis, releasing macrophage–resident microbes to be killed by other immune mechanisms (2). The current paradigm is that there are individual, receptor–specific inflammasomes consisting of one NLR (nucleotide-binding-and-oligomerization domain and leucine-rich-repeat-containing) or PYHIN (pyrin domain and HIN domain-containing) receptor, the adaptor protein apoptosis-associated speck-like protein containing a CARD (ASC), and caspase-1 (3). How the protein constituents of the inflammasome are spatially orientated is unclear.

NLRC4 and NLRP3 are the best characterized inflammasomes, especially with respect to their responses to pathogenic bacteria. The NLRC4 inflammasome is activated primarily by bacteria, including *Aeromonas veronii* (4), *Escherichia coli* (5), *Listeria monocytogenes* (6, 7), *Pseudomonas aeruginosa* (5), *Salmonella enterica* serovar Typhimurium (5, 8-10) and *Yersinia* species (11). In mouse macrophages, the NLRC4 inflammasome responds to flagellin and Type III secretion system (T3SS)–associated needle or rod proteins (5, 8, 9) after their detection by NAIP5 or NAIP6 and NAIP1 or NAIP2, respectively (12-15). Phosphorylation of NLRC4 at a single, evolutionarily conserved residue, Ser 533, by PRKCD (PKCδ) kinase is required for NLRC4 inflammasome assembly (16). The NLRP3 inflammasome is activated by a large repertoire of DAMPs, including ATP, nigericin, maitotoxin, uric acid crystals, silica, aluminium hydroxide and muramyl dipeptide (17-20). NLRP3 is also activated by bacterial PAMPs from many species, including *Aeromonas* species (4, 21), *L. monocytogenes* (6, 7, 22), *Neisseria gonorrhoe* (23), *S.* Typhimurium (10), *Streptococcus pneumoniae* (24) and *Yersinia* species (11). The mechanisms by which NLRC4 and NLRP3 inflammasomes contribute to host defense against bacterial pathogens are emerging, however, little is known about the dynamics governing inflammasome assembly in infections caused by bacteria that activate multiple NLRs, such as *S.* Typhimurium (10), *A. veronii* (4) and *Yersinia* (11).

NLRP3 does not have a CARD (caspase activation and recruitment domain) and requires ASC to interact with the CARD domain of procaspase-1. This interaction requires a charged interface around Asp27 of the procaspase-1 CARD (25). Whether ASC is also required for the assembly of the NLRC4 inflammasome is less clear. NLRC4 contains a CARD which can interact directly with the CARD domain of procaspase-1 (26), however ASC is required for some of the responses driven by NLRC4 (27). Macrophages infected with *S.* Typhimurium or other pathogens exhibit formation of a distinct cytoplasmic ASC focus or speck, which can be visualized under the microscope and is indicative of inflammasome activation (10, 28, 29). Our lab and others have shown that only one ASC speck is formed per cell irrespective of the stimulus used (29-32). Yet many bacteria activate two or more NLRs and it is unclear whether a singular inflammasome is formed at a time or multiple inflammasomes are formed independently of each other, with each inflammasome containing one member of the NLR family.

In this study we describe the endogenous molecular constituents of the *Salmonella*-induced inflammasome and their spatial orientation. In cross section, ASC forms a large external ring with the NLRs and caspases located internally. Critically NLRC4, NLRP3, caspase-1 and caspase-8 co-exist in the same ASC speck to coordinate pro-IL-1β processing. All ASC specks observed contained both NLRC4 and NLRP3. These results suggest that *Salmonella* infection induces a single inflammasome protein complex containing different NLRs and recruiting multiple caspases to co-ordinate a multifaceted inflammatory response to infection.

RESULTS

NLR and caspase-1 are both spatially organized within the *Salmonella*-induced ASC speck

The inflammasome adaptor protein ASC aggregates and forms a large speck in response to different inflammasome stimuli. Using confocal imaging we immunolocalized ASC after infection of primary bone marrow–derived macrophages (BMMs) with *S.* Typhimurium (MOI 10) for 1 h. ASC redistributed to form a focus or speck in BMMs infected with *S.* Typhimurium **(Fig. 1A)**, whereas endogenous ASC predominately distributed throughout the cytosol of unstimulated BMMs **(Fig. S1A)**. Each infected cell contained one ASC speck of 0.6–0.7 μm diameter after infection with *S.* Typhimurium **(Fig. 1A)**. Protein oligomerization assays confirmed that ASC

formed oligomers following *Salmonella* infection **(Fig. 1B)**. Specks that appeared in a cross section orientation had an apparent hole in the middle **(Fig. 1A)**. A similar ASC "ring" structure was observed in human THP-1 macrophages **(Fig. 1C and Fig. S1B).** We used Bayesian localization super-resolution microscopy to obtain higher magnification images of the specks in cross section (33). After infection of THP-1 cells or BMMs with *S*. Typhimurium (MOI 10) for 30 min, immuno-labeled ASC specks from different cells were visualized and the images compared to each other. Analysis of multiple cross sections of an ASC speck revealed that it forms a ring-like structure **(Fig. 1D).** Immuno-labeling of ASC using two different antibodies revealed the same ring-like structure **(Fig. S1C)**, suggesting that this is not due to the effect of a particular antibody. Further analysis of the ASC specks showed the presence of side filaments frequently decorating the external region of the ASC ring structure **(Fig. 1E).**

How other endogenous proteins of the inflammasome associate with and spatially distribute relative to ASC is unclear. We used super-resolution microscopy to resolve the spatial orientation of ASC, caspase-1, and either NLRP3 or NLRC4 in macrophages infected with *S.* Typhimurium. Confocal imaging of caspase-1 using FLICA labeling in THP-1 cells or mouse BMMs identified caspase-1 specks of a smaller diameter (0.426 μm +/- 0.047 μm; n=8) to the ASC specks **(Fig. 1C–E and Fig. S1D)**. Super-resolution imaging of ASC and caspase-1 colocalization showed that the ASC ring surrounded caspase-1, with the caspase-1 filling the central "hole" of the ASC ring **(Fig. 1C–E and Fig. S1D)**. We attempted to generate a three dimensional reconstruction of the super resolution ASC structure, however, the point spread function of the microscope is symmetric, which means that it is not possible to discriminate between point spread functions which are out-of-focus above the plane of focus, and those that are an equal distance low. However, we were able to discriminate between in-focus and out-of-focus point spread functions in the super resolution data. These show the in-focus fluorophores tending to be localized to the edge of the ring, with the out-of-focus fluorophores being more spread out **(Fig. S2)**. This suggests that the outer ring structure is reasonably well defined in one plane, with some degree of narrowing occurring above or below.

We next wondered how individual NLRs would spatially associate with ASC. LPS primed THP-1 cells were infected with *S*. Typhimurium for 30 min at MOI 10 and immuno-labeled for endogenous NLRP3 and ASC. Confocal imaging of NLRP3 showed, like those seen for caspase-1,

specks that were smaller (0.4 μm) than those seen with ASC immuno-labeling **(Fig. 2A)**. Super-resolution imaging of the co-labeled ASC and NLRP3 showed that NLRP3 formed a smaller ring-like structure within the ASC ring **(Fig. 2A)**. This technique also showed that diffused caspase-1 predominantly localized within the NLRP3 ring-like speck in infected BMMs **(Fig. 2B)**. Super-resolution microscopy of immuno-labeled NLRC4 also revealed smaller specks (0.578 μm +/- 0.079 μm; n=8) than those formed by ASC **(Fig. 2C and Fig. S3)**. Caspase-1 predominantly localized in a NLRC4 ring-like speck **(Fig. 2C)**. Immunolocalization of NLRP3 and ASC in the nigericin-stimulated canonical NLRP3 inflammasome produced a similar pattern to that observed in the *Salmonella*-induced inflammasome structure **(Fig S4)**. We confirmed our colocalization findings in HEK293 cells transfected with DNA constructs encoding different inflammasome proteins **(Fig. S5 and S6)**. Taken together we provide evidence to show that following *Salmonella* infection of macrophages endogenous NLRC4 or NLRP3 reside in the ASC speck, within which caspase-1 is located to form an inflammasome complex.

Co-ordinated activation of NLRs sustains infection-induced IL-1β production

NLRC4 and NLRP3 can both be activated by *Salmonella* (10), but the dynamics of how NLRC4 and NLRP3 activation is coordinated with respect to their localization within the ASC speck during infection is unclear. Infection of BMMs from wildtype and *Asc*$^{-/-}$ mice with log phase–grown wildtype *S.* Typhimurium for 2 h showed that *Salmonella* induction of caspase-1 proteolysis, pro-IL-1β processing and IL-1β release required ASC **(Fig. S7)**. Both NLRC4 and NLRP3 were required to drive robust IL-1β production **(Fig. 3A).** To further investigate the dynamics of NLRC4 and NLRP3-mediated IL-1β production, we infected primary BMMs from wildtype, *Nlrc4*$^{-/-}$ or *Nlrp3*$^{-/-}$ mice with *S.* Typhimurium lacking flagellin (Δ*fliC* Δ*fljB*), PrgJ (Δ*prgJ*) or all known activators of the NLRC4 inflammasome (Δ*fliC* Δ*fljB* Δ*prgJ*) (14, 15). We found that NLRC4 predominately drove caspase-1 proteolysis, pro-IL-1β processing and IL-1β production in response to all *Salmonella* mutants after 2 h of infection, whereas NLRP3 responded to all mutants following 24 h of infection **(Fig. 3B, 3C)**. Our results suggest that NLRC4 and NLRP3 cooperate to induce robust inflammasome activation following infection with *S.* Typhimurium.

Our *in vitro* data suggest a role for both NLRC4 and NLRP3 in the host response to infection with *S.* Typhimurium. In lethal salmonellosis NLRP3 and NLRC4 are required to control the infection on day 5 post-infection (10), but the relative contributions of these NLRs in regulating

bacterial burden over time is unknown. We therefore used a sublethal model of murine salmonellosis where the mice control bacterial growth and eventually clear the infection over time, which allows us to monitor the impact of NLRs on *Salmonella* growth over a longer time course. Mice were infected with *S.* Typhimurium and killed at days 1, 7 and 13 post-infection. A similar bacterial burden was found in all mice at day 1 **(Fig. 4)**. At day 7, both *Nlrc4*$^{-/-}$ or *Nlrp3*$^{-/-}$ mice had higher bacterial counts than wildtype mice **(Fig. 4)**. *Casp-1*$^{-/-}$(*casp-11*$^{-/-}$) mice had the highest bacterial burden compared to other mice on day 7, suggesting that both NLRs contribute to the host defense against *Salmonella* infection 7 days post-infection. On day 13, we observed elevated bacterial burden in *Nlrc4*$^{-/-}$ or *Nlrp3*$^{-/-}$ mice compared to wildtype mice **(Fig. 4)**. Unlike day 7, a substantially higher bacterial numbers were found in *Nlrc4*$^{-/-}$ mice compared to *Nlrp3*$^{-/-}$ mice on day 13. *Casp-1*$^{-/-}$(*casp-11*$^{-/-}$) mice still contained the highest bacterial burden compared to both *Nlrc4*$^{-/-}$ or *Nlrp3*$^{-/-}$ mice. These results suggest that the relative contribution between NLRC4 and NLRP3 in the host control of sub-lethal salmonellosis is comparable on day 7, whereas on day 13 NLRC4 exerts a greater antibacterial effect than NLRP3. The reason why we see distinct roles for NLRC4 and NLRP3, in comparison to Broz and colleagues (10), is simply because the differences in bacterial growth only become apparent as the infection progresses over time. This can only be seen if the animals can ultimately control bacterial growth. These data support the concept that NLRC4 and NLRP3 coordinate suppression of bacterial growth *in vivo* during *Salmonella* infection.

Multiple NLRs and caspases can be recruited to the same *Salmonella*-induced inflammasome

Activation of multiple NLRs in response to *Salmonella* infection occurs *in vitro* and *in vivo,* yet how is this achieved if cells only form a single inflammasome per cell? Infection of BMMs with *S.* Typhimurium for 24 h to induce the activation of both NLRC4 and NLRP3 still resulted in the formation of a single ASC speck per macrophage **(Fig. 5A).** A possible explanation for this is that triggering the formation of a single ASC speck by multiple NLRs could result in more than one NLR being present in the same inflammasome complex. Rather than having separate NLRP3 or NLRC4 inflammasomes occurring, we hypothesized that the inflammasome could be a single dynamic protein complex that is formed in response to different NLR inputs. NAIPs and NLRC4 are recruited to the same inflammasome so it is feasible that NLRP3 and NLRC4 may also be

present in a single inflammasome complex (14, 15). To investigate this, we used super-resolution microscopy to visualize immuno-labeled endogenous NLRC4 and NLRP3 in LPS-primed THP-1 macrophages infected with *S.* Typhimurium. All of the ASC specks observed contained both NLRC4 and NLRP3 and image analysis of these showed co-localization of both NLRs in the same speck **(Fig. 5B)**. NLRC4 localized in a ring-like structure (ring diameter 0.658 μm +/- 0.056 μm; n=10) whilst NLRP3 formed a smaller and more centralized ring-like structure (ring diameter 0.489 μm +/- 0.029 μm; n=10) **(Fig. 5C)**. We confirmed these findings by co-expressing DNA constructs encoding human NLRC4 and NLRP3 in HEK293 cells and found that both receptors redistributed and colocalized into a single complex **(Fig. S8)**. Our data suggest that NLRC4 and NLRP3 can be located to the same inflammasome.

Given that the inflammasome platform can contain more than one NLR we wondered whether this also occurs for inflammasome-associated caspases. We have previously shown that the ASC speck is required to recruit the inflammasome effectors, caspase-1 and caspase-8, into a single complex during *Salmonella* infection **(Fig. S9A)** (32). In THP-1 cells super-resolution analysis of the ASC-caspase-8 speck showed a similar distribution to that seen for caspase-1 distribution within the ASC ring, with the diameter of the caspase-8 core measured at 0.422 μm +/- 62 μm (n=7) **(Fig. 6A,B)**. We performed additional cross-sectional analysis of the ASC-Caspase-8 specks **(Fig. 6B)** and confirmed these findings in primary BMMs (**Fig. S9B).** Taken together, we hypothesized that a single inflammasome platform provides a major proteolytic cleavage site within the cell where pro-IL-1β must be recruited for processing. We stained pro-IL-1β, ASC and caspase-1 and found that pro-IL-1β formed a smaller speck-like structure (0.4 μm) that colocalized within the ASC-caspase-1 speck **(Fig. S10)**, suggesting that pro-IL-1β may be required to enter the inflammasome "pore" for proteolytic processing. It is not unreasonable to speculate that the ASC speck is a substrate-specific entity whereby only specific substrates such as pro-IL-1β and pro-IL-18 are able to enter for caspase-1 and -8–dependent processing while providing a controlled environment to prevent unregulated caspase-1 and -8 activity within the cell. The concentric organization of the speck suggests that ligand-mediated NLR activation provides a nucleation point for the rapid recruitment of ASC dimers and the subsequent assembly of the ASC speck, concomitant with the recruitment of caspase-1 and -8 **(Fig. 6C)**. This results in the formation of an inflammasome platform containing more than one NLR family member which

drives the recruitment of multiple effectors to the same protein complex to process pro-IL-1β and pro-IL-18.

DISCUSSION

Bacterial infection activates different NLRs to drive inflammasome production of IL-1β and IL-18 in the host tissue to help control the spread of the organism. Here we provide an answer to a central question in inflammasome biology. That is, in response to pathogens, like *Salmonella*, which activate multiple NLRs why does only a single ASC speck form? Our combined confocal and super-resolution imaging approach along with functional analysis shows, for the first time, that endogenous NLRC4 and NLRP3 colocalize in the same speck. Different NLRs can therefore be present in the same ASC speck to coordinate inflammasome functions after *Salmonella* infection. A single ASC speck can also contain multiple caspase effectors (caspase-1 and -8) at the same time, suggesting that the inflammasome platform is a dynamic protein complex that contains multiple NLRs and recruits more than one effector caspase to control the production of IL-1β.

Our work provides a clear picture of the gross organization of the endogenous ASC speck. The concentric organization of an external ASC layer surrounding the NLR proteins, which in turn surround the effector caspases, provides important insight into the function of the inflammasome. This arrangement permits the dynamic recruitment and movement of speck constituents following activation, thereby ensuring the inflammasome remains functionally active. For example, NLRP3 is critical for sustained pro-IL-1β processing and is recruited to the ASC speck at a later time point than NLRC4, which is instead crucial during early infection. Hence, NLRP3 is positioned inside NLRC4 **(Fig. 5B).** The formation of an outer shell of ASC, rather than a solid or closed speck, is also consistent with continual dynamic recruitment and with the presence of a functional core consisting of active caspases and pro-IL-1β **(Fig. S10)**. A core that would be inaccessible if the ASC formed a closed shell. The outer ASC shell may also serve to stabilize and protect the internal structure. It is interesting to note that side filaments are often found decorating the ASC shell although the functional significance of this is currently unclear.

The nature of the protein-protein interactions within the speck remains elusive at this resolution and it is intriguing that direct co-localization of components that reportedly interact is not always observed. This is likely to be a result of both the experimental reagents available and the functional organization of the speck. We predominantly co-stain ASC and active caspase-1 or -8 in our study, resulting in detection of active caspase-1/8 in the functional centre of the speck, pre-

sumably following its release from ASC **(Fig. 6)**. Whereas where we stained ASC and caspase-8 using an antibody that detects both cleaved and pro-forms, more of the caspase is localized with the ASC ring **(compare Fig. S9B and Fig. 6)**.

Our results show that the spatial orientation of NLRP3 and ASC in the nigericin-stimulated canonical inflammasome resembles a similar pattern to that observed in the more complex *Salmonella*-induced inflammasome structure **(Fig S4).** We speculate that the composition of the AIM2 inflammasome would have a similar structure to the multi-NLR inflammasome. Indeed, analysis of the crystal structure of the HIN200 domain of AIM2 and dsDNA revealed that the positively charged HIN domain embraces the dsDNA while the AIM2 PYD domain located periphery to the HIN-dsDNA structure is thought to facilitate the recruitment of ASC (34). This proposed structure composed of dsDNA-AIM2 internal to ASC is similar to our observed structure comprised of NLRC4 and NLRP3 within an ASC shell. In contrast to our concentric ring structure where caspase-1 lies within the ASC ring, a recent study using Cryo-EM analysis suggests that caspase-1 forms filamentous structures external to ASC following nucleation by either NLRP3 or AIM2 (35). This difference is most likely due to the altered protein levels between an exogenous over-expression system and our own visualization of the endogenous inflammasome. Earlier EM-staining of endogenous ASC also reports a hollow, ring-like organization (36). The cryo-EM analysis of the AIM2 ternary complex and the NLRP3 inflammasome represents a snapshot of inflammasome formation and may correlate with the starting point of full speck formation. This would be followed by additional NLR and ASC recruitment leading ultimately to the ring-like structure we observe.

Salmonella activates both NLRC4 and NLRP3 which results in ASC focus formation and recruitment of caspases to the inflammasome (10, 32). Our data show that *in vitro* NLRP3 contributes to the macrophage response against *Salmonella* at a later stage than NLRC4 in unprimed conditions. This is unsurprising as NLRP3 expression in BMMs requires induction by LPS or cytokines such as TNF-α (37). In experiments using unprimed BMMs infected with *Salmonella* **(Fig 2A and B)**, there will be a delay before NLRP3 is expressed, whereas NLRC4, which is constitutively expressed, will be activated immediately upon cellular infection. *In vivo* as infection progresses the effect of NLRC4 is slightly more important at day 13 in comparison to days 1 and 7. There are many factors that could explain the differences, including time-dependent effects of NLRC4 and NLRP3 *in vitro* and *in vivo*. These include the changing profile of cytokines,

the effects of NLRC4, but not NLRP3, in driving *Salmonella*-induced pyroptosis, and the switch in cell type dominance, over time during infection. Macrophages, for example, play a key role at day 7, the time point at which NLRC4 and NLRP3 have a similar effect *in vivo*, whereas by day 13 other cells such as NK cells and $CD4^+$ T cells are starting to play a major role in controlling the infection.

If NLRC4 and NLRP3 both contribute to the host defense against *Salmonella* infection, then mice lacking either of these receptors should show a greater susceptibility to *Salmonella* infection compared to wildtype mice. Our work supports this hypothesis because mice lacking NLRC4 or NLRP3 have higher bacterial loads than the wildtype mice at days 7 and 13 post-infection. Broz *et al* (10) previously reported that mice lacking NLRC4 or NLRP3 harbor similar bacterial numbers in the spleen, liver and mesenteric lymph nodes 5 days after *Salmonella* infection, however, consistent with our observations, they showed that mice lacking both NLRP3 and NLRC4 harbor a higher bacterial load compared to wildtype controls. We observed similar bacterial numbers in spleen and liver between wildtype mice and any of the knock-out strains at an early time point (day 1), but as the infection progresses (days 7 and 13) we see a clear increase in the bacterial burden in mice lacking NLRC4 or NLRP3. This observation highlights an important role for each of these receptors over the course of *Salmonella* infection, which is consistent with our *in vitro* data.

Our data lead us to propose that the inflammasome is a dynamic multi-protein complex, where NLRC4, NLRP3, caspase-1, caspase-8 and pro-IL-1β co-localize to the same ASC inflammasome in macrophages infected with *Salmonella*. Whether caspase-11 might associate with ASC in the non-canonical inflammasome is unclear and the spatial distribution of these proteins will be an interesting area for future research. In conclusion, our data reveal cooperative interactions between distinct members of the NLR and caspase families that form a dynamic inflammasome during *Salmonella* infection.

MATERIALS AND METHODS

Detailed information is presented in SI Materials and Methods. We used Bayesian localization microscopy to obtain super-resolution images of the ASC inflammasome structure (33). Super-

resolution experiments were performed on a Nikon TI eclipse inverted microscope using a Nikon intensilight light source for fluorescence.

ACKNOWLEDGEMENTS

We would like to thank K.A. Fitzgerald (University of Massachusetts Medical School, USA) for critical review of our manuscript and for supplying the knockout mouse strains, G. Núñez (University of Michigan Medical School, USA) for the anti-NLRC4 antibody, and E. Creagh (Trinity College Dublin, Ireland) for providing technical advice and the ASC construct, F. Morgan, S. Achouri and I. Kazanis (University of Cambridge, UK) for providing assistance in microscopy. S.M.M was supported by a Cambridge International Scholarship. T.P.M was supported by a Wellcome Trust Research Career Development Fellowship (WT085090MA). This study was supported by Biotechnology and Biological Sciences Research Council (BBSRC) grants (BB/H003916/1 and BB/K006436/1) and a BBSRC Research Development Fellowship (BB/H021930/1) awarded to C.E.B.

REFERENCES

1. Franchi L, Muñoz-Planillo R, & Núñez G (2012) Sensing and reacting to microbes through the inflammasomes. *Nat Immunol* 13(4):325-332.
2. Miao EA, *et al.* (2010) Caspase-1-induced pyroptosis is an innate immune effector mechanism against intracellular bacteria. *Nat Immunol* 11(12):1136-1142.
3. Rathinam VAK, Vanaja SK, & Fitzgerald KA (2012) Regulation of inflammasome signaling. *Nat Immunol* 14(4):333-342.
4. McCoy AJ, Koizumi Y, Higa N, & Suzuki T (2010) Differential regulation of caspase-1 activation via NLRP3/NLRC4 inflammasomes mediated by aerolysin and type III secretion system during *Aeromonas veronii* infection. *J Immunol* 185(11):7077-7084.
5. Miao EA, *et al.* (2010) Innate immune detection of the type III secretion apparatus through the NLRC4 inflammasome. *Proc Natl Acad Sci U S A* 107:3076-3080.
6. Wu J, Fernandes-Alnemri T, & Alnemri ES (2010) Involvement of the AIM2, NLRC4, and NLRP3 inflammasomes in caspase-1 activation by *Listeria monocytogenes*. *J Clin Immunol* 30(5):693-702.
7. Meixenberger K, *et al.* (2010) *Listeria monocytogenes*-infected human peripheral blood mononuclear cells produce IL-1beta, depending on listeriolysin O and NLRP3. *J Immunol* 184(2):922-930.
8. Miao EA, *et al.* (2006) Cytoplasmic flagellin activates caspase-1 and secretion of interleukin 1beta via Ipaf. *Nat Immunol* 7(6):569-575.

9. Franchi L, *et al.* (2006) Cytosolic flagellin requires Ipaf for activation of caspase-1 and interleukin 1beta in salmonella-infected macrophages. *Nat Immunol* 7(6):576-582.
10. Broz P, *et al.* (2010) Redundant roles for inflammasome receptors NLRP3 and NLRC4 in host defense against *Salmonella*. *J Exp Med* 207(8):1745-1755.
11. Brodsky IE, *et al.* (2010) A *Yersinia* effector protein promotes virulence by preventing inflammasome recognition of the type III secretion system. *Cell Host Microbe* 7(5):376-387.
12. Yang J, Zhao Y, Shi J, & Shao F (2013) Human NAIP and mouse NAIP1 recognize bacterial type III secretion needle protein for inflammasome activation. *Proc Natl Acad Sci U S A* 110(35):14408-14413.
13. Rayamajhi M, Zak DE, Chavarria-Smith J, Vance RE, & Miao EA (2013) Cutting Edge: Mouse NAIP1 Detects the Type III Secretion System Needle Protein. *J Immunol* 191(8):3986-3989.
14. Kofoed EM & Vance RE (2011) Innate immune recognition of bacterial ligands by NAIPs determines inflammasome specificity. *Nature* 477(7366):592-595.
15. Zhao Y, *et al.* (2011) The NLRC4 inflammasome receptors for bacterial flagellin and type III secretion apparatus. *Nature* 477(7366):596-600.
16. Qu Y, *et al.* (2012) Phosphorylation of NLRC4 is critical for inflammasome activation. *Nature* 490(7421):539-542.
17. Li H, Willingham SB, Ting JP, & Re F (2008) Cutting edge: inflammasome activation by alum and alum's adjuvant effect are mediated by NLRP3. *J Immunol* 181(1):17-21.
18. Mariathasan S, *et al.* (2006) Cryopyrin activates the inflammasome in response to toxins and ATP. *Nature* 440(7081):228-232.
19. Dostert C, *et al.* (2008) Innate immune activation through Nalp3 inflammasome sensing of asbestos and silica. *Science* 320(5876):674-677.
20. Hornung V, *et al.* (2008) Silica crystals and aluminum salts activate the NALP3 inflammasome through phagosomal destabilization. *Nat Immunol* 9(8):847-856.
21. McCoy AJ, *et al.* (2010) Cytotoxins of the human pathogen *Aeromonas hydrophila* trigger, via the NLRP3 inflammasome, caspase-1 activation in macrophages. *Eur J Immunol* 40(10):2797-2803.
22. Kim S, *et al.* (2010) *Listeria monocytogenes* is sensed by the NLRP3 and AIM2 inflammasome. *Eur J Immunol* 40(6):1545-1551.
23. Duncan JA, *et al.* (2009) *Neisseria gonorrhoeae* activates the proteinase cathepsin B to mediate the signaling activities of the NLRP3 and ASC-containing inflammasome. *J Immunol* 182(10):6460-6469.
24. McNeela EA, *et al.* (2010) Pneumolysin activates the NLRP3 inflammasome and promotes proinflammatory cytokines independently of TLR4. *PLoS Pathog* 6(11):e1001191.
25. Kersse K, Lamkanfi M, Bertrand MJ, Vanden Berghe T, & Vandenabeele P (2011) Interaction patches of procaspase-1 caspase recruitment domains (CARDs) are differently involved in procaspase-1 activation and receptor-interacting protein 2 (RIP2)-dependent nuclear factor kappaB signaling. *J Biol Chem* 286(41):35874-35882.
26. Poyet JL, *et al.* (2001) Identification of Ipaf, a human caspase-1-activating protein related to Apaf-1. *J Biol Chem* 276(30):28309-28313.
27. Proell M, Gerlic M, Mace PD, Reed JC, & Riedl SJ (2013) The CARD plays a critical role in ASC foci formation and inflammasome signalling. *Biochem J* 449(3):613-621.

28. Jones JW, *et al.* (2010) Absent in melanoma 2 is required for innate immune recognition of *Francisella tularensis*. *Proc Natl Acad Sci U S A* 107(21):9771-9776.
29. Huang MT, *et al.* (2009) Critical role of apoptotic speck protein containing a caspase recruitment domain (ASC) and NLRP3 in causing necrosis and ASC speck formation induced by *Porphyromonas gingivalis* in human cells. *J Immunol* 182(4):2395-2404.
30. Fernandes-Alnemri T, *et al.* (2007) The pyroptosome: a supramolecular assembly of ASC dimers mediating inflammatory cell death via caspase-1 activation. *Cell Death Differ* 14(9):1590-1604.
31. Broz P, von Moltke J, Jones JW, Vance RE, & Monack DM (2010) Differential requirement for Caspase-1 autoproteolysis in pathogen-induced cell death and cytokine processing. *Cell Host Microbe* 8(6):471-483.
32. Man SM, *et al.* (2013) *Salmonella* infection induces recruitment of Caspase-8 to the inflammasome to modulate IL-1beta production. *J Immunol* 191(10):5239-5246.
33. Cox S, *et al.* (2011) Bayesian localization microscopy reveals nanoscale podosome dynamics. *Nat Methods* 9(2):195-200.
34. Jin T, *et al.* (2012) Structures of the HIN domain:DNA complexes reveal ligand binding and activation mechanisms of the AIM2 inflammasome and IFI16 receptor. *Immunity* 36(4):561-571.
35. Lu A, *et al.* (2014) Unified Polymerization Mechanism for the Assembly of ASC-Dependent Inflammasomes. *Cell* 156(6):1193-1206.
36. Masumoto J, *et al.* (1999) ASC, a novel 22-kDa protein, aggregates during apoptosis of human promyelocytic leukemia HL-60 cells. *J Biol Chem* 274(48):33835-33838.
37. Bauernfeind FG, *et al.* (2009) Cutting edge: NF-kappaB activating pattern recognition and cytokine receptors license NLRP3 inflammasome activation by regulating NLRP3 expression. *J Immunol* 183(2):787-791.

FIGURE LEGENDS

Fig. 1 Spatial organization of the ASC speck.
(A) Immuno-labeling of endogenous ASC in primary bone marrow-derived macrophages (BMMs) infected with *S.* Typhimurium (*S*Tm). (B) Endogenous ASC oligomerized in unprimed or LPS-primed BMMs following *S*Tm infection. (C) Confocal microscopy imaging of endogenous immuno-labeled ASC and FLICA staining of caspase-1 in human THP-1 macrophages infected with *S*Tm. (D) Bayesian localization super-resolution microscopy of endogenous ASC and caspase-1 in C. (E) Multiple cross-sections of the ASC–Caspase-1 speck. Arrows indicate side filaments of ASC coming off the external region of the ring-like structure.

Fig. 2 NLRs reside in the ASC speck following *S.* Typhimurium infection of macrophages.
Bayesian localization super-resolution microscopy of (A) endogenous immuno-labeled ASC and NLRP3, (B) endogenous immuno-labeled NLRP3 and FLICA-stained caspase-1 and (C) endogenous immuno-labeled NLRC4 and FLICA-stained caspase-1 in human THP-1 macrophages infected with *S.* Typhimurium.

Fig. 3 Co-ordinated activation of NLRs is required for IL-1β production induced by *S.* Typhimurium infection. WT, *Nlrc4*$^{-/-}$ and *Nlrp3*$^{-/-}$ primary bone marrow-derived macrophages (BMMs) were infected with (A) *S.* Typhimurium SL1344 or (B) its isogenic mutants Δ*fliC*, Δ*fljB*, Δ*fliC*Δ*fljB*, Δ*prgJ* and Δ*fliC*Δ*fljB*Δ*prgJ* (multiplicity of infection [MOI] 1) for the indicated times. (A,B) Supernatant (SN) was collected and the levels of IL-1β were measured using ELISA. (C) Pro-caspase-1, cleaved caspase-1 p10, pro-IL-1β and cleaved IL-1β p17 were detected in the supernatant or cell lysate using western blotting. β-actin was used as a loading control. Data shown are representatives of two (C) and three (A,B) experiments.

Fig. 4 NLRC4 and NLRP3 have non-redundant roles in the host defense against sub-lethal murine *S.* Typhimurium (STm) infection. WT, *Nlrc4*$^{-/-}$, *Nlrp3*$^{-/-}$ and *casp-1*$^{-/-}$(*casp-11*$^{-/-}$) mice were infected intravenously (i.v) with 1.33×10^4 CFUs *S*Tm strain M525P (a strain that establishes sub-lethal murine salmonellosis) and the mean bacterial load was determined in the spleen and liver after 1, 7 and 13 days of infection. Three to four animals of each genotype were

used per group per time point. Data are from one set of experiment representative of two. ns, no statistical significance, ** $P < 0.01$ and *** $P < 0.001$.

Fig. 5 NLRC4 and NLRP3 are recruited to the same *Salmonella*-induced ASC speck.
(A) Unprimed WT primary bone marrow-derived macrophages (BMMs) were infected with *S.* Typhimurium (*S*Tm) expressing green fluorescent protein (GFP) for 2 or 24 h, and stained for ASC and DNA. The number of ASC foci per infected BMM was counted. At least 180 infected BMMs (indicated by the presence of GFP-expressing *S*Tm) were counted in each of the four independent experiments. (B) Bayesian localization super-resolution microscopy of endogenous NLRC4 and NLRP3 in THP-1 macrophages infected with *S*Tm. (C) Image analysis of the ring diameter of the NLRC4 and NLRP3 structures in B (n=10).

Fig. 6 Caspase-8 is recruited to the same *Salmonella*-induced ASC speck. (A,B) Bayesian localization super-resolution microscopy of endogenous immuno-labeled ASC and FLICA-stained caspase-8 in THP-1 macrophages infected with *S.* Typhimurium. (B) Multiple cross-sections of the ASC–Caspase-8 speck. Arrows indicate side filaments of ASC. Image analysis of the ring diameter of the ASC and caspase-8 structures (n=7). (C) A schematic of ASC speck assembly in response to *Salmonella* infection in a macrophage.

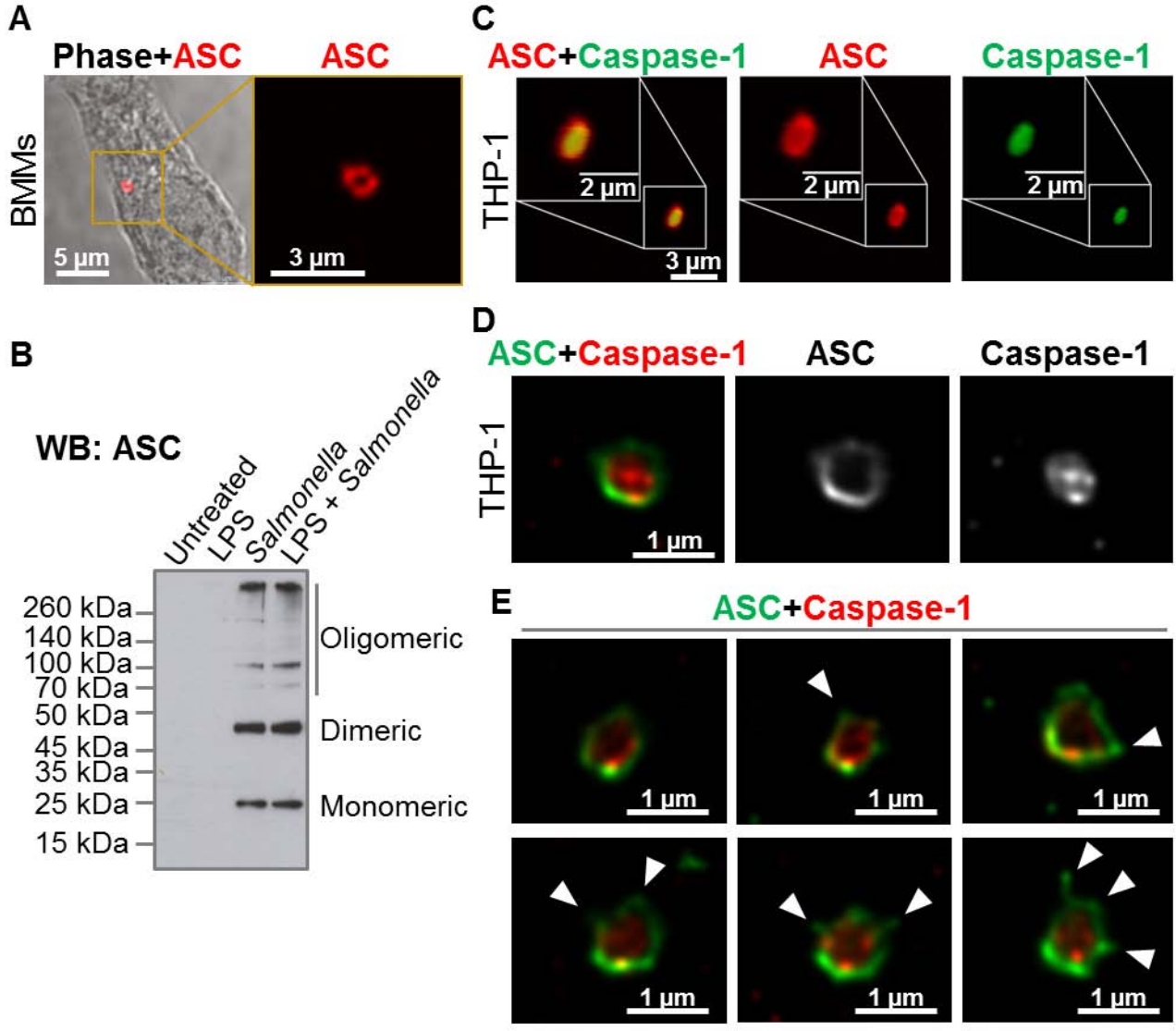
A
Phase+ASC
ASC
BMMs
5 μm
3 μm
C
ASC+Caspase-1
ASC
Caspase-1
THP-1
2 μm
3 μm
B
WB: ASC
Untreated
LPS
Salmonella
LPS + Salmonella
260 kDa
140 kDa
100 kDa
70 kDa
50 kDa
45 kDa
35 kDa
25 kDa
15 kDa
Oligomeric
Dimeric
Monomeric
D
ASC+Caspase-1
ASC
Caspase-1
THP-1
1 μm
E
ASC+Caspase-1
1 μm

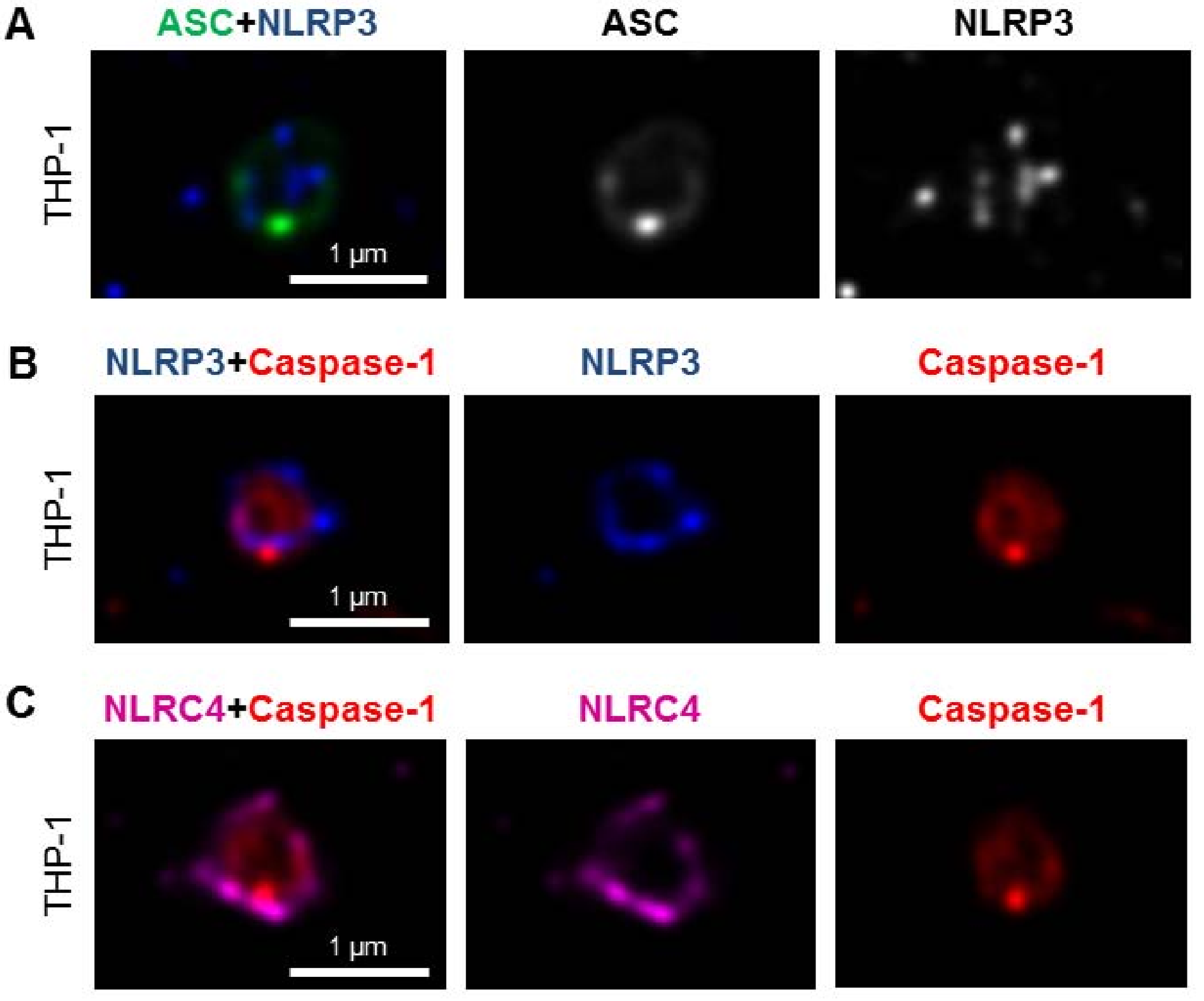
A
ASC+NLRP3
ASC
NLRP3
THP-1
1 μm
B
NLRP3+Caspase-1
NLRP3
Caspase-1
THP-1
1 μm
C
NLRC4+Caspase-1
NLRC4
Caspase-1
THP-1
1 μm

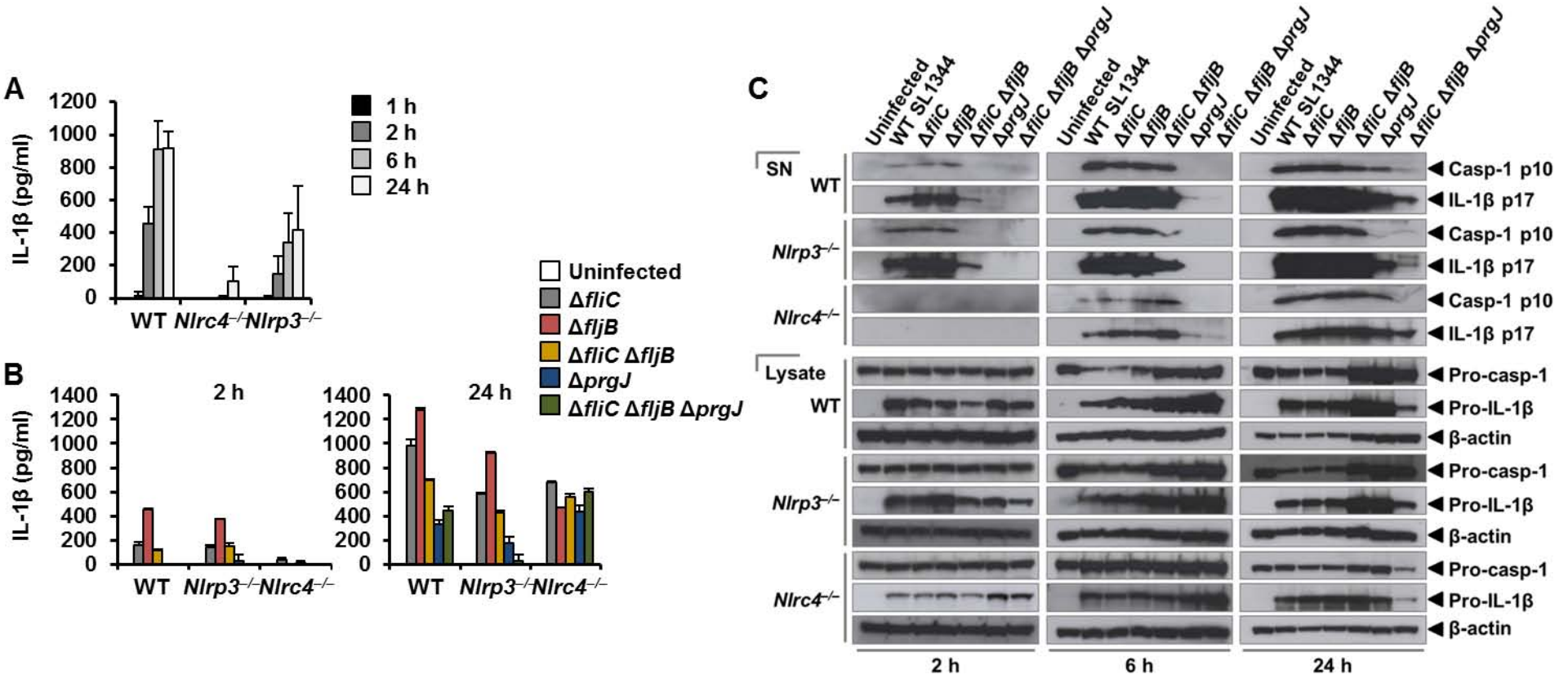
A
IL-1β (pg/ml)
1200
1000
800
600
400
200
0
WT
Nlrc4−/−Nlrp3−/−
1 h
2 h
6 h
24 h
B
IL-1β (pg/ml)
2 h
24 h
WT
Nlrp3−/−Nlrc4−/−
Uninfected
ΔfliC
ΔfljB
ΔfliC ΔfljB
ΔprgJ
ΔfliC ΔfljB ΔprgJ
C
Uninfected
WT SL1344
ΔfliC
ΔfljB
ΔfliC ΔfljB
ΔprgJ
ΔfliC ΔfljB ΔprgJ
SN
Lysate
WT
Nlrp3−/−
Nlrc4−/−
Casp-1 p10
IL-1β p17
Pro-casp-1
Pro-IL-1β
β-actin
2 h
6 h
24 h

Day 1 (i.v)
Day 7 (i.v)
Day 13 (i.v)
Log10 CFU/spleen
Log10 CFU/liver
ns
**
***
Wild-type
Nlrp3-/-
Nlrc4-/-
Casp-1-/-(11-/-)

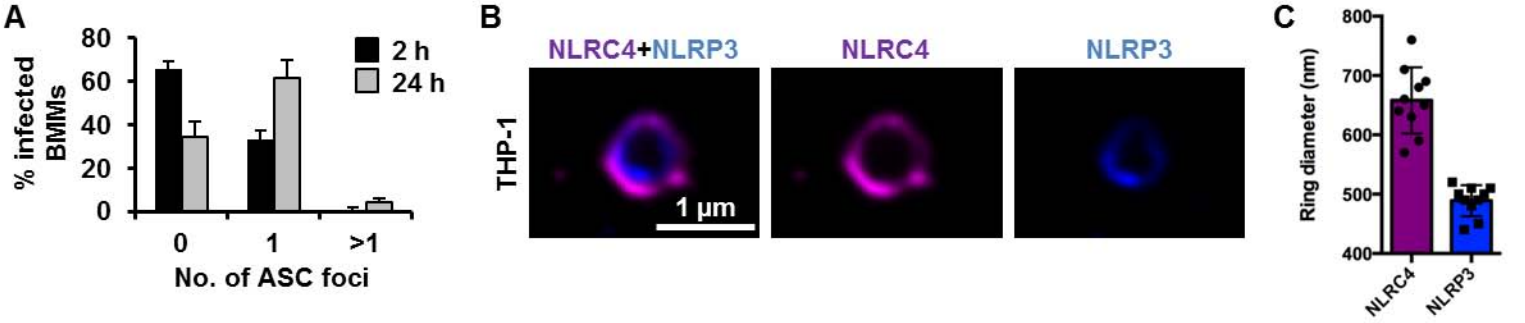
A
% infected BMMs
80
60
40
20
0
2 h
24 h
0
1
>1
No. of ASC foci
B
NLRC4+NLRP3
NLRC4
NLRP3
THP-1
1 µm
C
Ring diameter (nm)
800
700
600
500
400
NLRC4
NLRP3

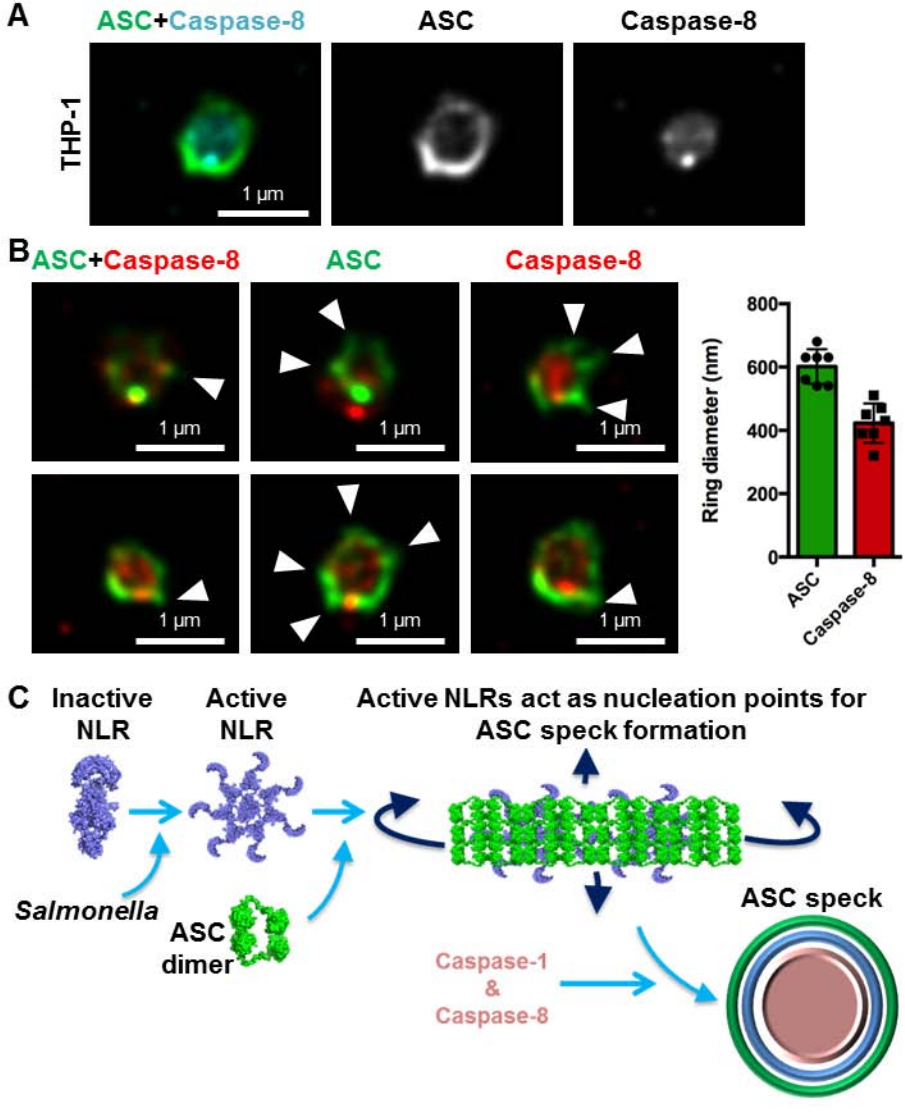
A
ASC+Caspase-8
ASC
Caspase-8
THP-1
1 µm
B
ASC+Caspase-8
ASC
Caspase-8
1 µm
Ring diameter (nm)
800
600
400
200
0
ASC
Caspase-8
C
Inactive NLR
Active NLR
Active NLRs act as nucleation points for ASC speck formation
Salmonella
ASC dimer
ASC speck
Caspase-1 & Caspase-8

Supporting Information

Materials and Methods

Mice and infection

Wildtype C57BL/6 mice (Harlan, Loughborough, UK), *Nlrc4*$^{-/-}$ mice, *Nlrp3*$^{-/-}$ mice, *Asc*$^{-/-}$ mice and *Caspase-1(-11)*$^{-/-}$ mice on the C57BL/6 background (all from Millennium Pharmaceuticals) were housed in a specific pathogen–free facility according to the Animals Scientific Procedures outlined by the UK Home Office regulations. Six- to eight-week-old mice were infected with *S.* Typhimurium strain M525P grown overnight at 37 °C in static culture in LB medium. Bacteria resuspended in PBS were injected into the tail veins of mice, and after 1, 7 and 13 days, killed by cervical dislocation. Spleens and livers were homogenized in a Colworth stomacher and the number of viable bacteria was determined by plating on LB agar.

Bacterial infection, ligand stimulation and inhibitor study on primary bone marrow derived macrophages

Primary bone marrow–derived macrophages (BMMs) were cultivated in DMEM with 5 mM L-glutamine (Sigma), 10% FCS (Hyclone), 20% L929 conditioned media and 10 μg/ml gentamicin (Sigma) for 5–6 days before use. BMM were seeded in antibiotic–free media at a concentration of 2×10^5 cells onto 96-well plates and incubated overnight. THP-1 monocytes were grown in RPMI 1640 supplemented with 10% FCS, 5 mM L-glutamine 1% penicillin and streptomycin (10,000 units/ml) and 20 μM 2-mercaptoethanol. THP-1 cells were differentiated in Phorbol 12-myristate 13-acetate–supplemented (250 nM, Sigma) media for 3 days. *S.* Typhimurium SL1344 was inoculated into LB broth and incubated for 17.5 h and subcultured (1:10) into fresh LB broth for 2 h. BMMs were infected with *S.* Typhimurium using the indicated Multiplicities of Infection (MOI). Bacteria were plated onto LB agar plates to confirm the number of inoculated bacteria. For 2 h infection, supernatant were removed after 1 h and replaced with media containing 50 μg/ml gentamicin (Sigma) for 1 h to kill extracellular bacteria. For 6 and 24 h infection, media containing 10 μg/ml gentamicin was used after 1 h incubation in media containing 50 μg/ml gentamicin. In experiments which required LPS priming, macrophages were stimulated using 200 ng/ml of ultrapure LPS

from *E. coli* (Invivogen) for 3 h. To activate the canonical NLRP3 inflammasome, 5 μM nigericin (Sigma) was used to stimulate cells for 30 min.

Cytokine measurement

Levels of mouse IL-1β secreted into the supernatant were measured using the BD OptEIA™ Mouse IL-1β Set according to the manufacturer's instructions.

Transfection

HEK293 cells were grown in DMEM (Sigma) supplemented with 10% FCS (Hyclone), 5 mM L-glutamine (Sigma) and penicillin and streptomycin (Sigma). Cells were seeded on cell-culture treated glass dishes (VWR) at a density of 2×10^5 cells. HEK293 cells were transfected the next day with constructs encoding human NLRC4-HA, NLRP3-FLAG, ASC-FLAG, Caspase-1 or with the empty vector pcDNA3. The ASC-FLAG construct was a gift from Emma Creagh (Trinity College Dublin, Ireland). Transfection was performed using 3 μl of Genejuice transfection reagent (Merck) per μg of DNA. Cells were incubated for 48 h.

Immunofluorescence staining

Macrophages or HEK293 cells were washed twice with PBS, fixed in -30 ˚C methanol for 5 min or 4% (w/v) paraformaldehyde for 15 min. Blocking was performed using 10% normal goat serum or rabbit serum (Dako) in 0.1% saponin (Sigma) for 1 h. Cells were stained with primary and secondary antibodies for 50 min or overnight and 40 min, respectively. The primary antibodies used were rabbit anti-ASC antibody (AL177; ENZO), mouse anti-mouse ASC antibody (clone 2EI-7; Millipore), rabbit anti-mouse cleaved caspase-8 (#5892; Cell Signaling Technology), goat anti-mouse IL1-β (AF-401-NA; R&D Systems), rabbit anti-human caspase-1 (sc-515; Santa Cruz Biotechnology) mouse anti-NLRP3 antibody (ALX-804-881-C100; ENZO), rabbit anti-NLRC4 (gift from Gabriel Núñez), goat anti-NLRP3 (ab4207; Abcam), mouse or rat anti-FLAG antibody (Sigma) and mouse or rabbit anti-HA antibody (Sigma). The secondary antibodies used were Alexa Fluor 488, 568 or 647, anti-rabbit, anti-mouse, anti-goat or anti-rat IgG (Invitrogen). Cells were counterstained in DAPI mounting medium (Vecta Labs). To stain for active caspases, the supernatant from macrophages was removed following stimulation and replaced with media which contain

0.5× reconstituted FLICA active caspase-1 (FAM-YVAD-FMK), caspase-8 (FAM-IETD-FMK) or polycaspases (FAM-VAD-FMK) reagents (immunochemistry) and incubated for an additional 1 h. Cells were then fixed in 4% (w/v) paraformaldehyde and stained as described above. Cells and inflammasomes were visualized, counted and imaged using the Leica DM6000 B fluorescence microscope or the Leica TCS SP5 confocal microscope.

Super-resolution microscopy

We used Bayesian localization microscopy (34) to obtain super-resolution images of the ASC inflammasome structure in fixed cells. Macrophages were washed twice with PBS and fixed in 4% (w/v) paraformaldehyde for 15 min. Cells were permeabilised with 0.2% TritonX-100 in PBS for 20 min. Blocking was performed using 1% BSA and 0.1% Triton X-100 in PBS for 30 min. Cells were stained with primary and secondary antibodies as outlined above in 1% BSA and 0.1% Triton X-100 in PBS for overnight and 1 h, respectively. Super-resolution experiments were performed on a Nikon TI eclipse inverted microscope using a Nikon intensilight light source for fluorescence. Cells were imaged through an oil immersion objective (×60, Numerical aperture 1.4) and a ×2.5 Nikon relay lens. Images were collected on a low-noise Andor iXon EMCCD camera (pixel pitch 16 μm) at a frame rate of 43 frames per second. We applied the Bayesian localization analysis to sequences of 300 frames, which corresponds to an acquisition time of 7s.

Western blotting

Proteins from cell culture supernatants were precipitated using the methanol–chloroform method as described.(20) Cell lysates were prepared by adding cell lysis buffer (150 mM NaCl, 50 mM Tris-HCl pH8, 1% Triton X-100, 1 mM PMSF, 10 μg/ml leupeptin, 1 μg/ml aprotinin) to cells and incubated for 10 min on ice before collecting the supernatant by centrifugation. Samples were separated by 4–20% gradient SDS–PAGE and transferred onto PVDF membranes. The primary antibodies used were rabbit anti-mouse caspase-1 p10 (sc-514; Santa Cruz Biotechnology), goat anti-mouse IL1-β (AF-401-NA; R&D Systems) and mouse anti-β-actin monoclonal antibody (ab3280; Abcam). The secondary antibodies used were goat anti-rabbit IgG-HRP, rabbit anti-goat IgG-HRP (sc-2004 and sc-2922, respectively; Santa Cruz Biotechnology) or polyclonal goat anti-mouse IgG-HRP (P0447; DAKO).

Statistical analysis

Statistical significance between values from two groups was determined using unpaired Student's t-test, and values between three or more groups was determined using One-way Analysis of Variance (ANOVA) with all values corrected using the Tukey-Kramer Multiple Comparisons Test (GraphPad Software). $P<0.05$ is considered significant.

SUPPLEMENTARY FIGURE LEGENDS

Fig. S1. Endogenous ASC forms a speck-like structure following *Salmonella* infection (related to Fig. 1). (A) Unprimed wildtype primary bone marrow–derived macrophages (BMMs) were stained for ASC (red) and DNA (blue). (B) Endogenous ASC redistributed to form a distinct 1-μm pore–shaped structure in THP-1 cells stimulated with intracellularly-delivered *Salmonella* flagellin. (C) Bayesian localization super-resolution microscopy of endogenous ASC immuno-labeled using two different antibodies from two different commercial suppliers in BMMs infected with *S*Tm. (D) The morphology of endogenous ASC–caspase-1 specks visualized by Bayesian localization super-resolution microscopy in primary mouse BMDMs infected with *S.* Typhimurium.

Fig. S2. Analysis of the in-focus and out-of-focus point spread functions of an ASC-caspase-1 speck using Bayesian localization microscopy. This analysis shows (A) the in-focus fluorophores tending to be localized to the edge of the ring, with (B) the out-of-focus fluorophores being more spread out.

Fig. S3. Caspase-1 is localized within a larger NLRC4 ring-like structure (related to Fig. 2). Image analysis of the ring diameter of the NLRC4 and caspase-1 structures observed by Bayesian localization super-resolution microscopy (n=8).

Fig. S4. NLRP3 resides in the ASC speck following stimulation of the canonical NLRP3 inflammasome in macrophages. Bayesian localization super-resolution microscopy of

endogenous immuno-labeled NLRP3 and ASC in human THP-1 macrophages stimulated with 5 μM of nigericin for 30 min.

Fig. S5. ASC and caspase-1 colocalize in a transfection system (related to Fig. 1). HEK293 cells transfected with hASC and hCaspase-1 DNA constructs. Cells were immuno-stained for the cytosolic distribution of these proteins.

Fig. S6. NLRs and ASC colocalize in a transfection system (related to Fig. 2.). (A) HEK293 cells transfected with hNLRP3 alone or with hNLRP3 and hASC DNA constructs. (B) HEK293 cells transfected with hNLRC4 alone or with hNLRC4 and hASC DNA constructs. (C) HEK293 cells transfected with hNLRC4 and hCaspase-1 DNA constructs. Cells were immuno-stained for the cytosolic distribution of these proteins.

Fig. S7. ASC is required for caspase-1 proteolysis in *Salmonella* infection (related to Fig. 3). Wildtype, *Asc* $^{-/-}$, *caspase-1* $^{-/-}$ (*caspase-11* $^{-/-}$) LPS-primed primary bone marrow–derived macrophages with *S.* Typhimurium (MOI 10) for 1 h. Cleaved IL-1β p17 subunit (processed IL-1β), cleaved caspase-1 p10 subunit (active caspase-1), pro-IL-1β, pro-caspase-1 and β-actin in the supernatant or cell lysate were detected by western blot analysis.

Fig. S8. NLRC4 and NLRP3 colocalize in a transfection system (related to Fig. 5). HEK293 cells transfected with hNLRC4 and hNLRP3 DNA constructs. Cells were immuno-stained for the cytosolic distribution of these proteins.

Fig. S9. Endogenous Caspase-8 is recruited to the same *Salmonella*-induced ASC speck (related to Fig. 6). (A) Confocal microscopy imaging of endogenous immuno-labeled ASC and FLICA staining of caspase-8 in human THP-1 macrophages infected with *S*Tm. (B) Bayesian localization super-resolution microscopy of endogenous immuno-labeled ASC and caspase-8 in primary mouse bone marrow-derived macrophages infected with *S*Tm. Multiple cross-sections of the ASC–Caspase-8 speck. Arrows indicate side filaments of ASC coming off the external region of the ring-like structure.

Fig. S10. The endogenous ASC speck recruits caspase-1 and pro-IL-1β. LPS-primed wildtype primary bone marrow–derived macrophages (BMMs) were infected with *S*Tm for 30 min in the presence of caspase-1 FLICA stain (Green) and immuno-stained for ASC (magenta), pro-IL-1β/IL-1β (red) and DNA (blue).

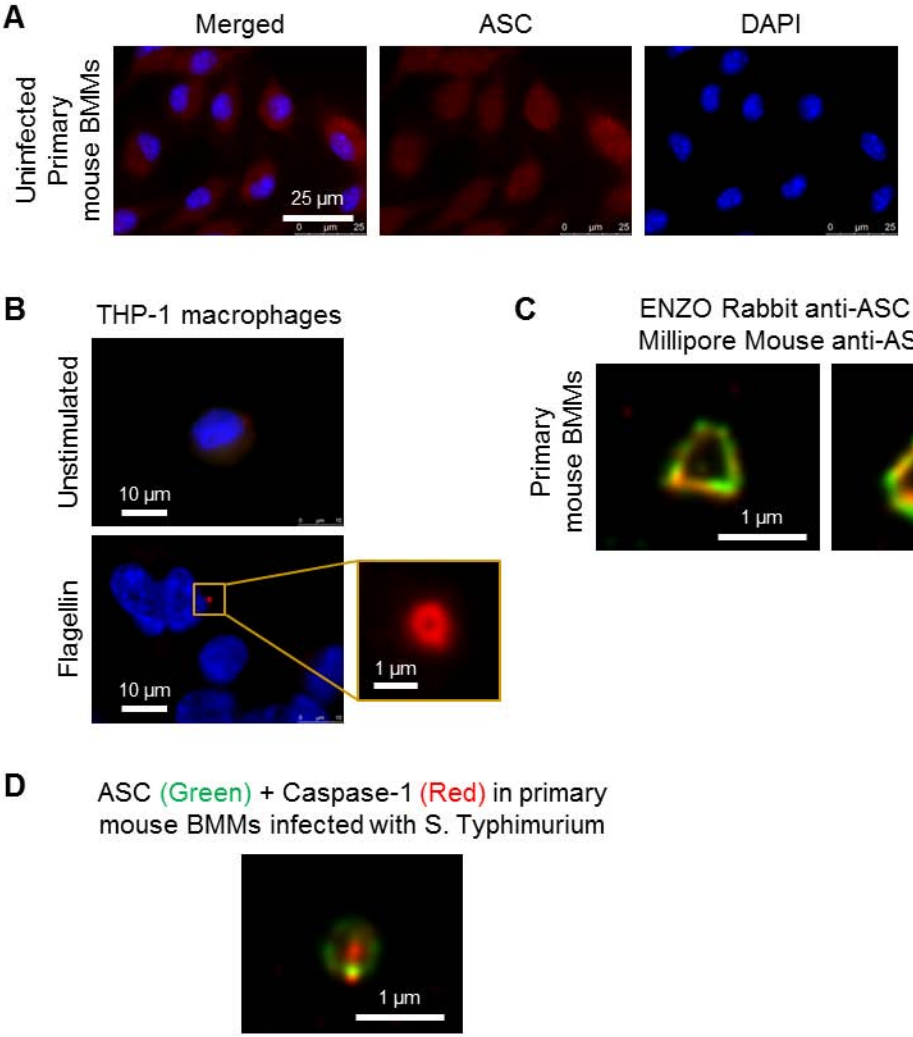

Supplementary Figure 1

A

ASC staining

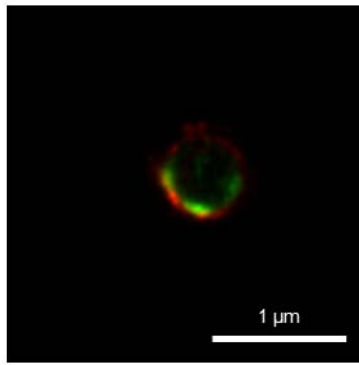

B

Caspase-1 staining

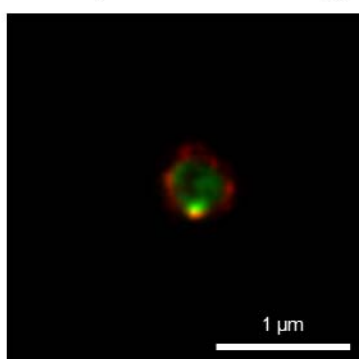

In-focus fluorophores (Red)
Out-of-focus fluorophores (Green)

Supplementary Figure 2

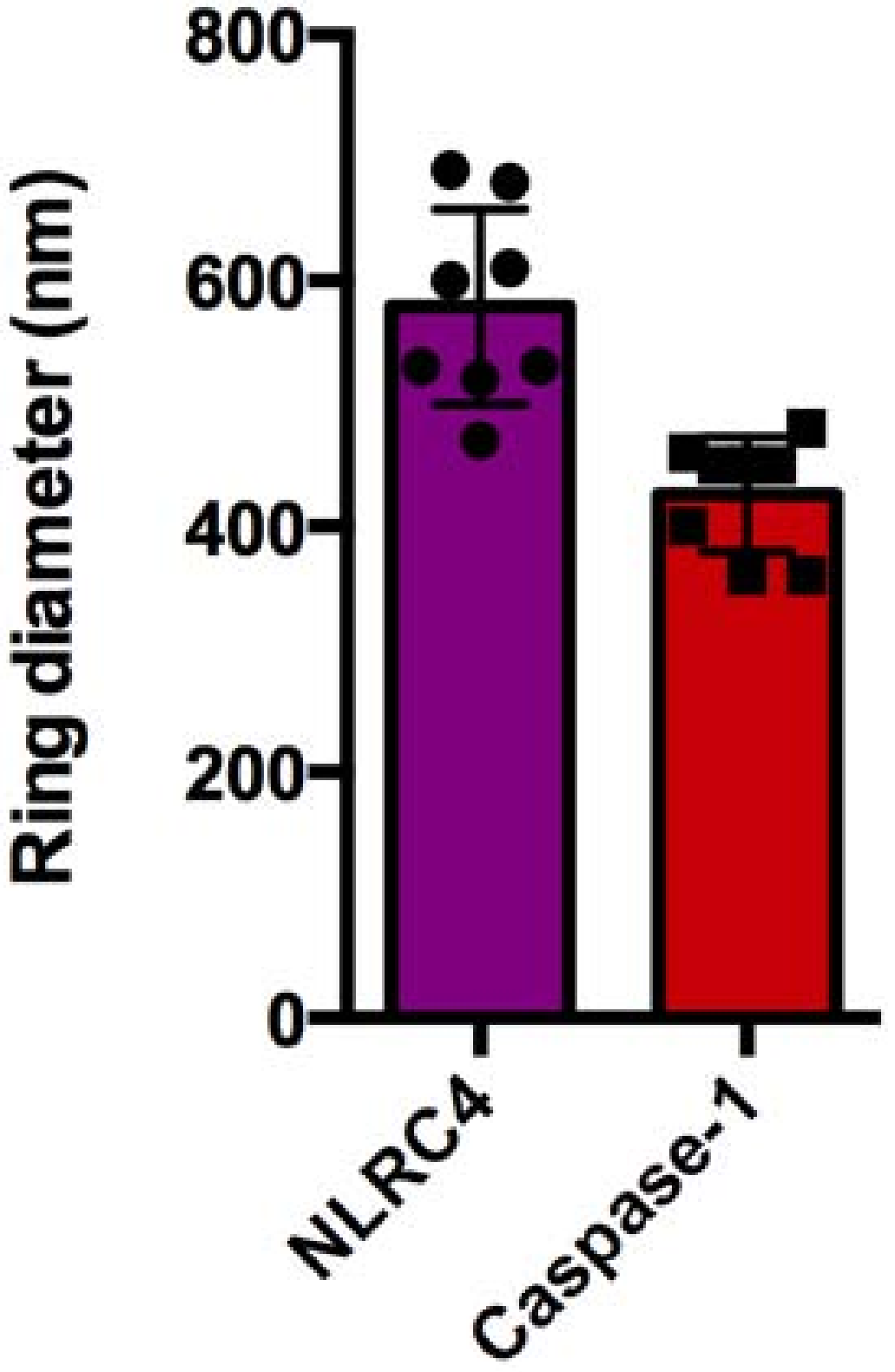

Supplementary Figure 3

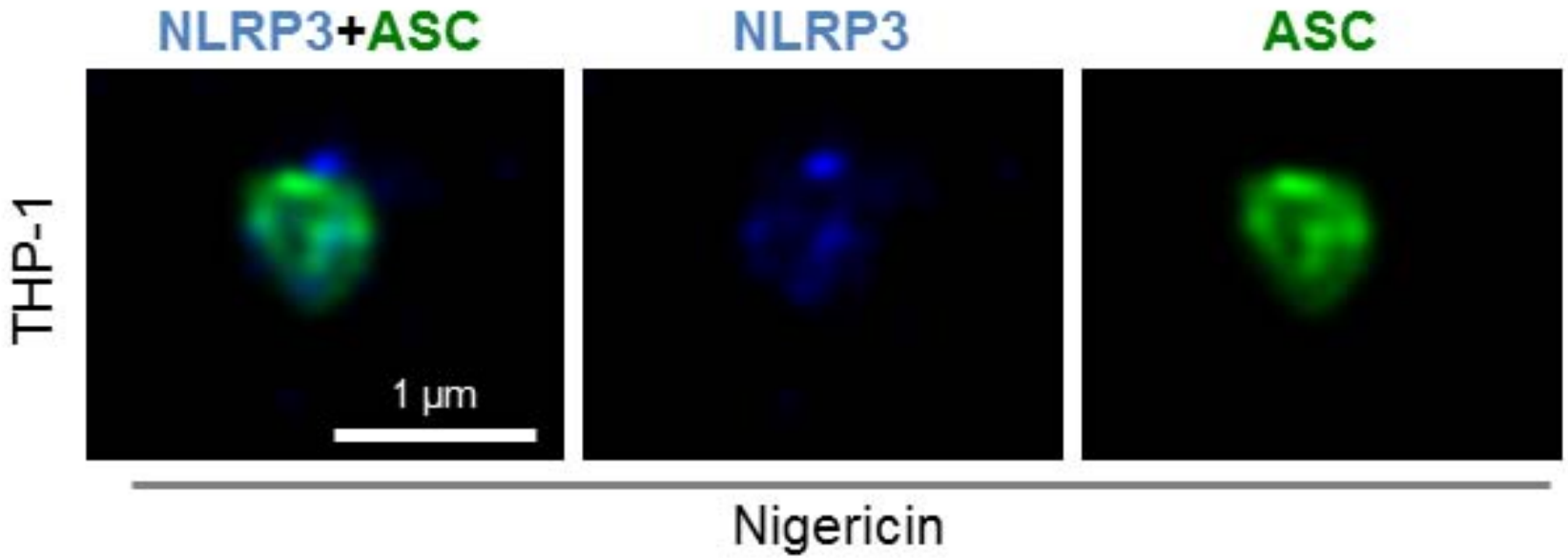

Supplementary Figure 4

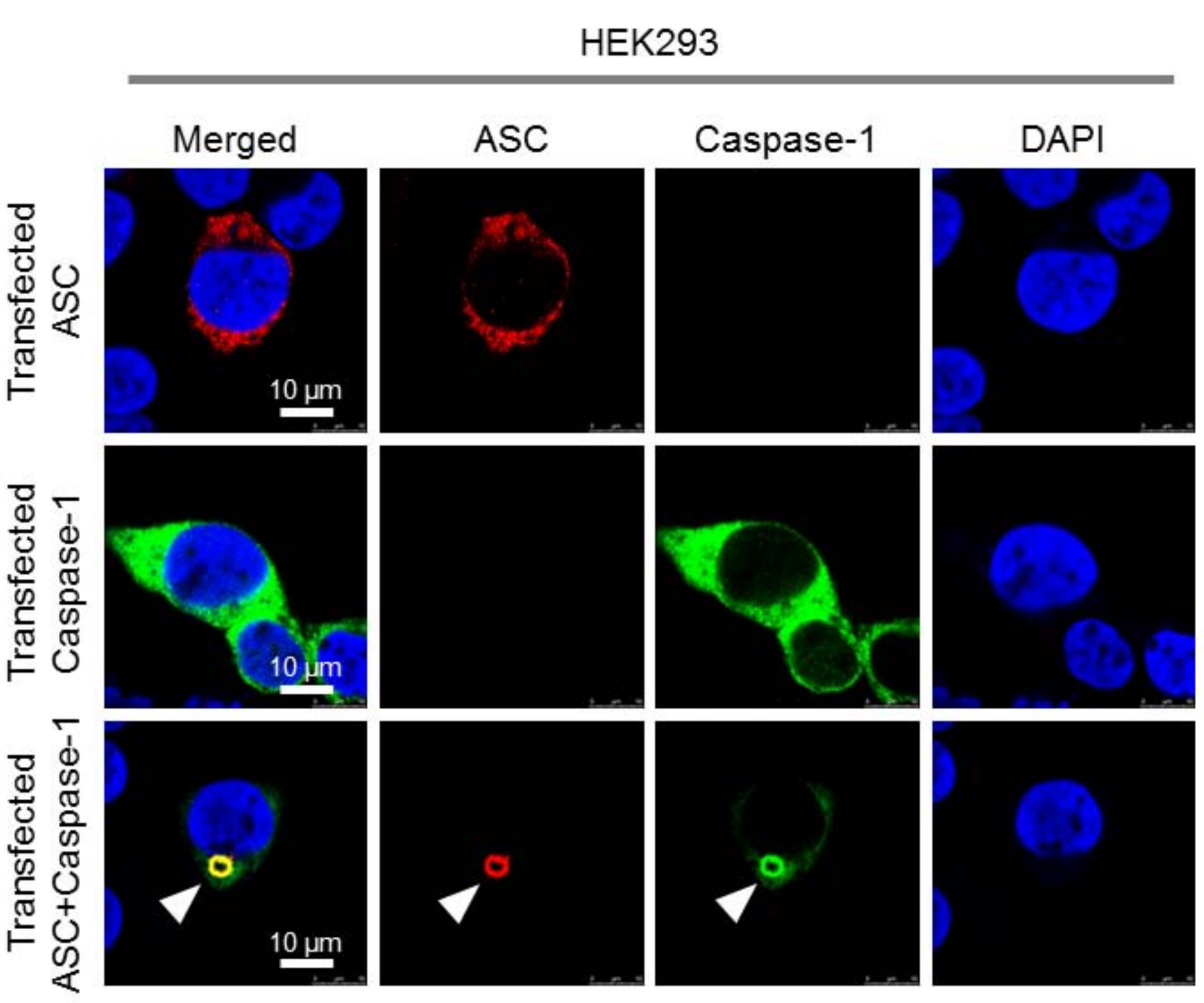

Supplementary Figure 5

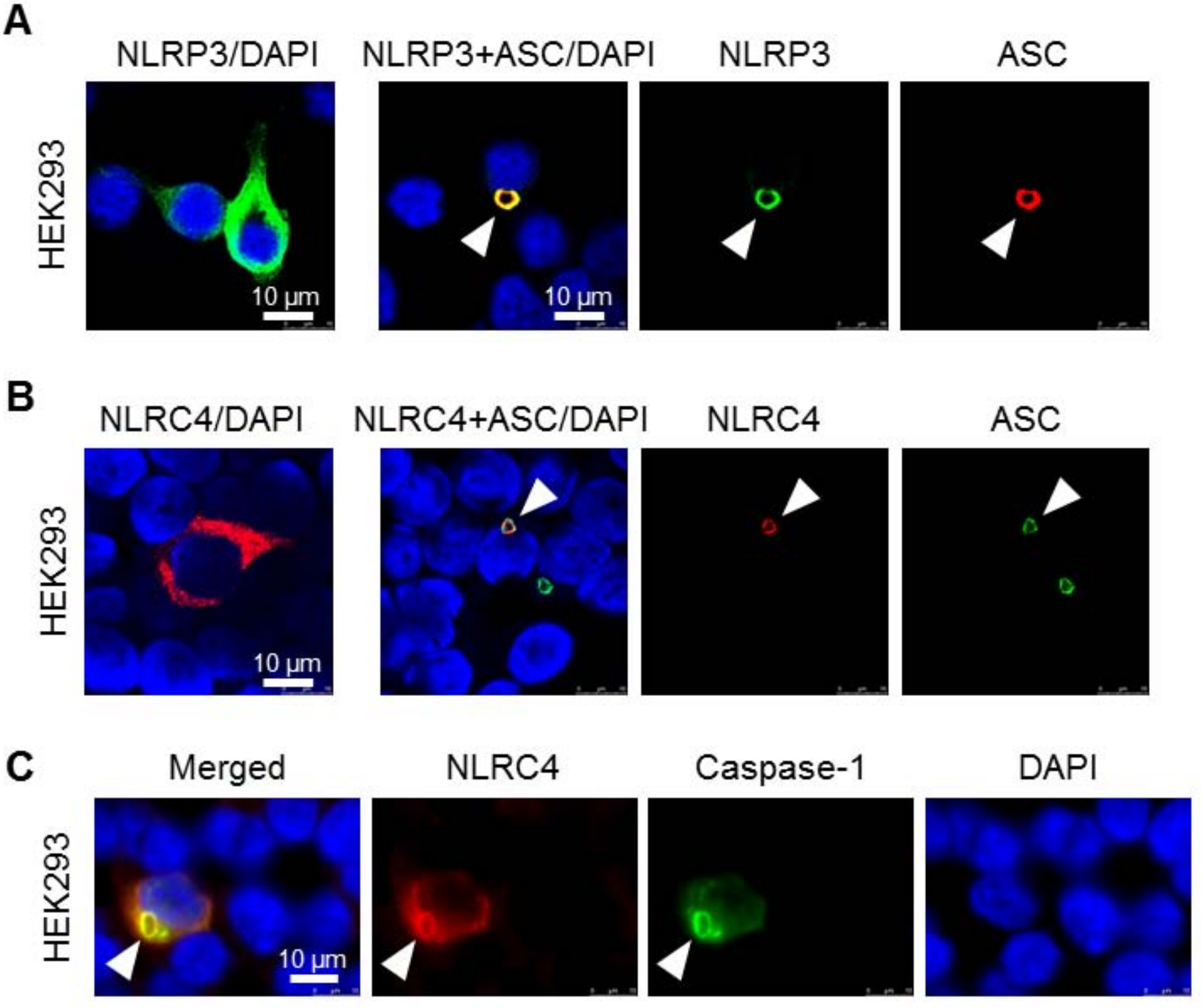

Supplementary Figure 6

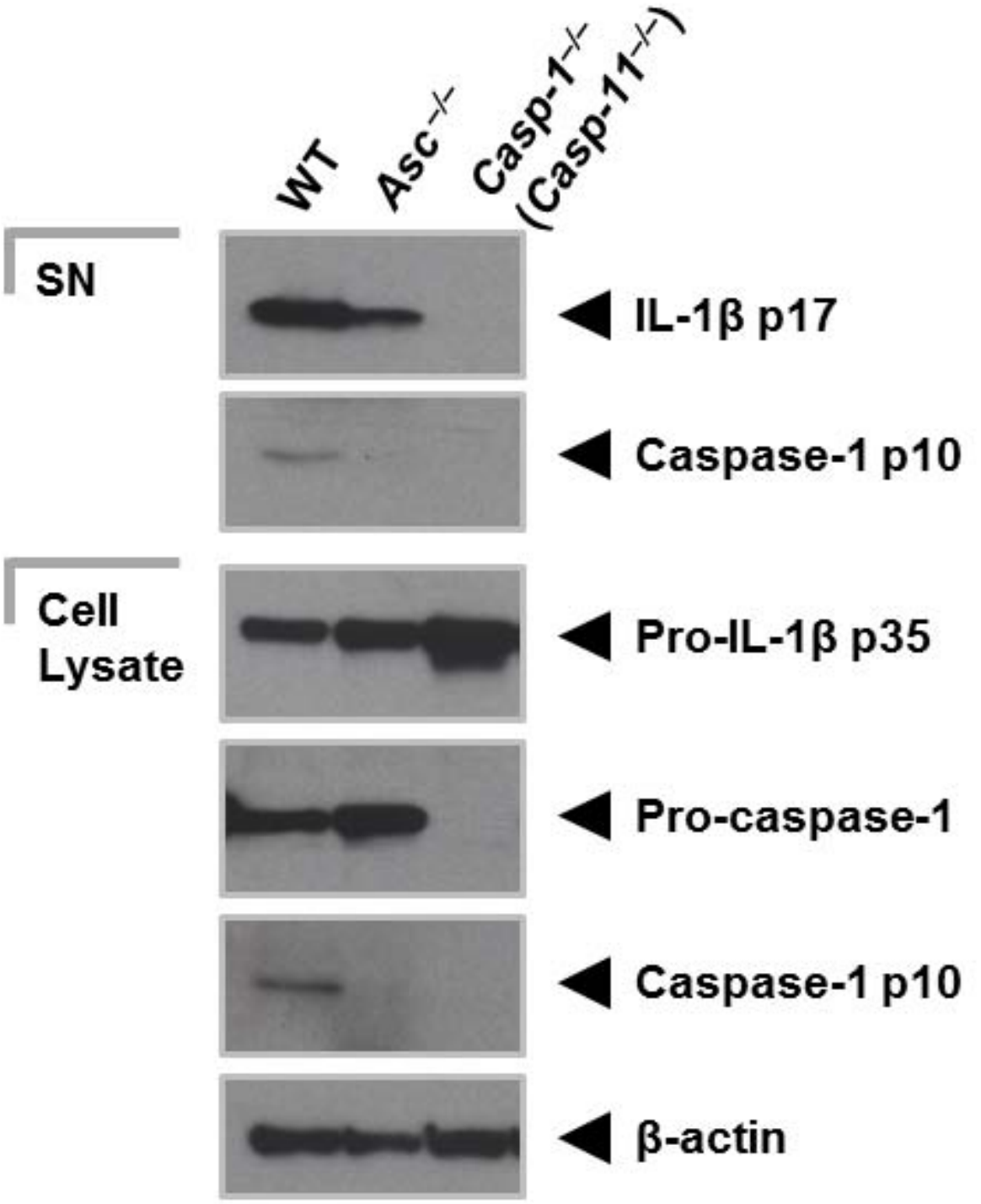

Supplementary Figure 7

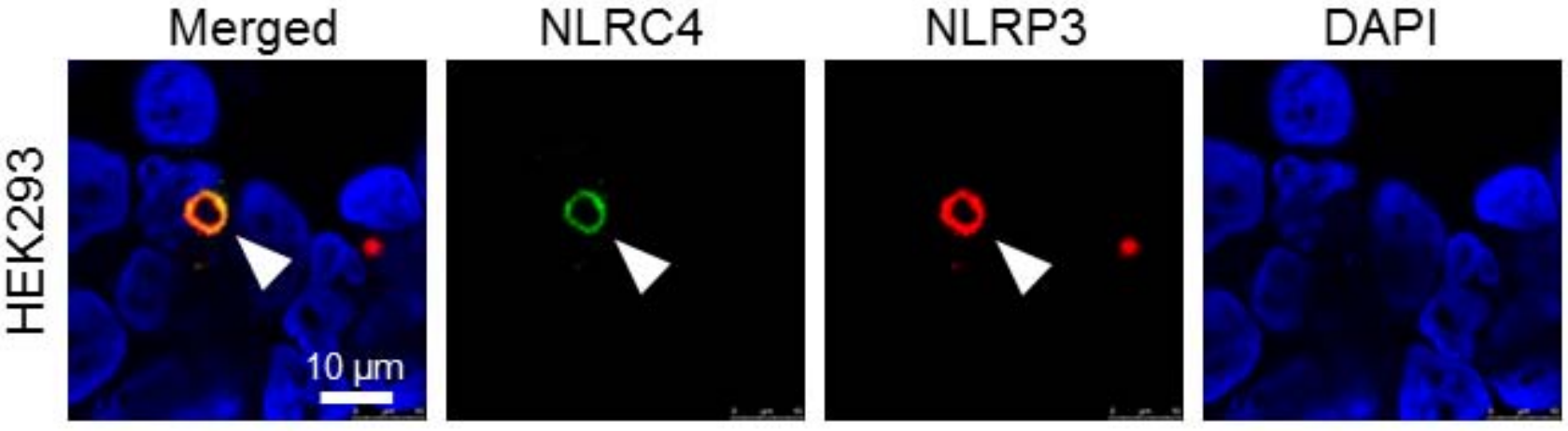

Supplementary Figure 8

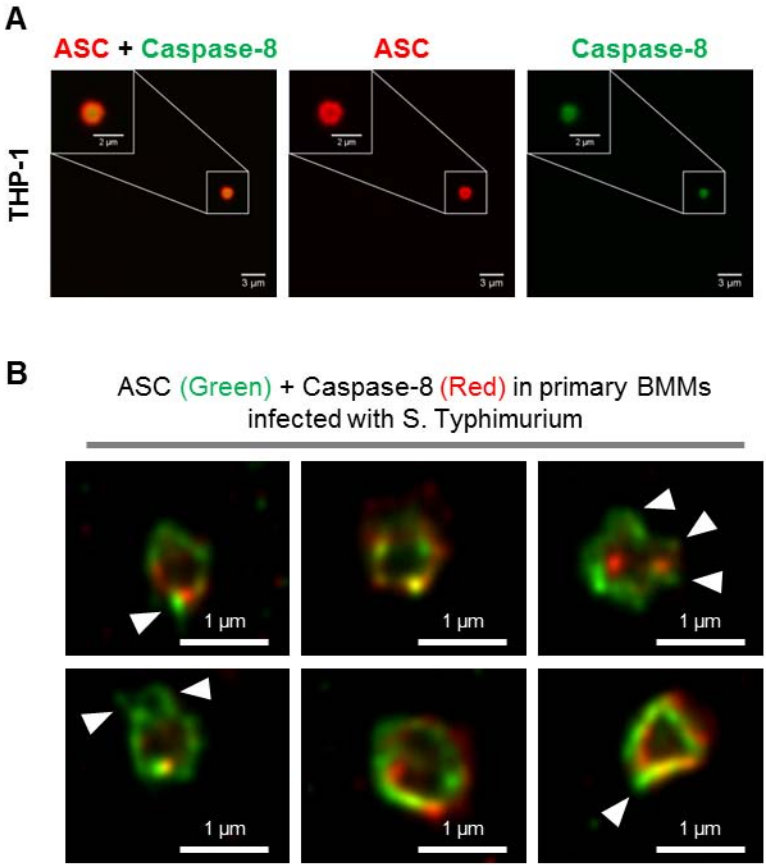

Supplementary Figure 9

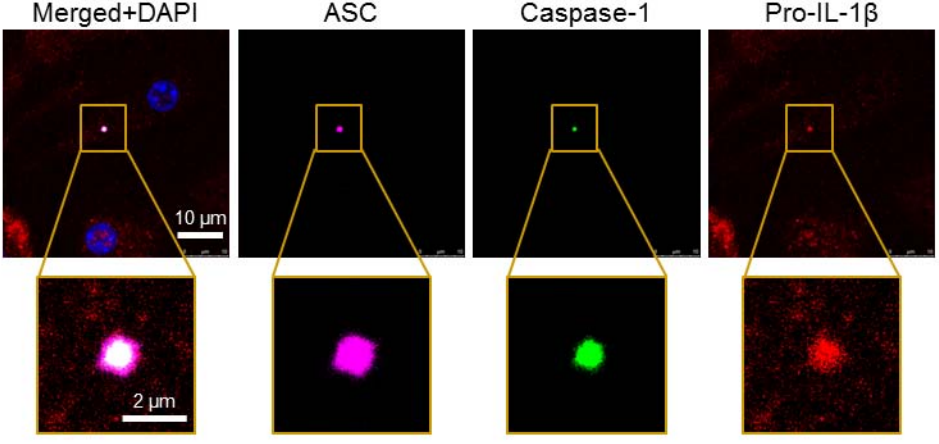

Supplementary Figure 10